

Soft topological modes protected by symmetry in rigid mechanical metamaterials

Hradesh Kedia,^{1,2} Anton Souslov,³ and D. Zeb Rocklin^{1,*}

¹*School of Physics, Georgia Institute of Technology, Atlanta, GA 30332*

²*Physics of Living Systems Group, Department of Physics,
Massachusetts Institute of Technology, Cambridge, MA 02139*

³*Department of Physics, University of Bath, Claverton Down, Bath BA2 7AY, UK*

Topological mechanics can realize soft modes in mechanical metamaterials in which the number of degrees of freedom for particle motion is finely balanced by the constraints provided by interparticle interactions. However, solid objects are generally hyperstatic (or overconstrained). Here, we develop a framework for how symmetries may be applied to generate topological soft modes even in overconstrained, rigid systems. To do so, we consider non-Hermitian topology based on non-square matrices. We then design hyperstatic materials in which low-energy modes protected by topology and symmetry appear at interfaces. Our approach presents a novel way of generating softness in robust scale-free architectures suitable for miniaturization to the nanoscale.

Topologically protected modes possess novel properties and extraordinary robustness stemming from their dual nature: these modes appear at the *boundaries*, yet are generated by *bulk* properties [1–7]. First realized in electronic states [7–11], this topological bulk-boundary correspondence has since been extended to the mechanics, acoustics, and photonics of structured matter [1–5, 12–29]. All of these systems are characterized by *topological invariants*, quantized numbers associated with a physical state. The type of invariants that a particular system can exhibit, or whether such topological character can exist at all, depends on its symmetries and has been classified for conventional, Hermitian Hamiltonians via the *tenfold way* [30]. More recently, topological concepts have been generalized to open quantum and classical systems in the presence of external drive and dissipation using fundamental ideas from non-Hermitian physics, which nevertheless focus on square Hamiltonians [6, 31–43].

For the mechanics of ball-and-spring networks, Ref. [44] predicts a number of localized floppy (zero-energy) modes proportional to a local flux of a bulk topological polarization. These topologically protected modes have been realized in mechanical metamaterials along interfaces in one, two, and three dimensions, as well as at dislocation defects [44–49]. These realizations require a fine balance (called isostaticity) between the numbers of degrees of freedom and constraints (e.g., springs) to define the underlying topological polarization. Isostaticity allows for this topological invariant by enforcing a one-to-one mapping between degrees of freedom at sites and the bonds between them. These distinct quantities can then be related via a non-Hermitian rigidity matrix (analogous to a Hamiltonian), which is square only for isostatic systems. However, isostatic materials are inherently unstable [50], which makes realizing isostatic topological lattices in atomic, molecular, or colloidal crystals especially challenging.

For the non-isostatic case, topologically protected soft

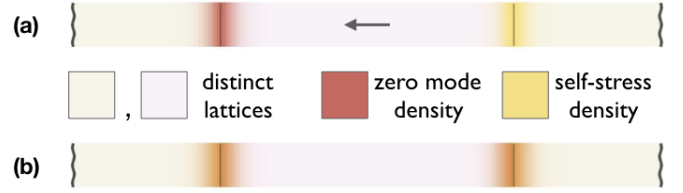


FIG. 1. (Color) Schematic illustration of the differences between topological mechanical phenomena in (a) Maxwell lattices without generalized inversion symmetry and (b) Maxwell lattices with generalized inversion symmetry. (a) In the absence of generalized inversion symmetry, Maxwell lattices can have topological polarization (shown by the grey arrow) and consequently have zero modes and self-stress states localized on opposite interfaces. (b) In the presence of generalized inversion symmetry, Maxwell lattices have no topological polarization and consequently have zero modes and self-stress states localized on the both interfaces.

modes are a consequence of topological invariants distinct from topological polarization. For example, overconstrained (i.e., hyperstatic) systems can possess low-dimensional topological boundary modes at the corners of two-dimensional systems [51]. For modes at interfaces (instead of corners), Ref. [52] includes an exhaustive classification scheme evocative of the tenfold way but for non-square non-Hermitian Hamiltonians, which could be applied to design non-isostatic systems.

Here we focus on mechanically stable lattices, which are overconstrained (i.e., hyperstatic), as are nearly all naturally occurring crystals. Although generically these crystals are not expected to have any soft modes, we show that a certain symmetry class can guarantee the presence of soft modes at any interface between topologically distinct states. We dub this the *generalized inversion symmetry* and demonstrate how to design both lattice geometries and interfaces between distinct configurations such that the symmetry is respected. Our work contributes to the understanding of non-Hermitian topology by extending design principles for topological modes beyond square Hamiltonians to rectangular matrices.

Generalized inversion symmetry—The linear deforma-

* zebrocllin@gatech.edu

tions of a mechanical system may be described via a *rigidity matrix* \mathcal{R} , a linear map determined from the system geometry that maps the displacements of sites (or more general degrees of freedom) onto the extensions of springs (or more general violations of constraints) and hence may be used to generate a potential energy. In real space, this rigidity matrix is real but not square. For periodic systems, the matrix can be written in Fourier space in terms of the wavenumber k , resulting in a block diagonal matrix with blocks $\mathcal{R}(k)$ as Laurent polynomials in the phase factor $\exp(ik)$ with real coefficients. Zero edge modes appear at complex wavenumbers k , for which the phase factor becomes a general complex number z [3, 53].

In the presence of an additional symmetry—generalized inversion symmetry—even lattices in which the number of constraints exceeds the number of degrees of freedom can be classified into topologically distinct states, see Ref. [52]. We define the generalized inversion symmetry by the existence of a basis in which $\mathcal{R}(k)$ is real for real wavenumbers k , i.e., that there exist unitary matrices U, W such that $U^\dagger \cdot \mathcal{R}(k) \cdot W \in \mathbb{R} \ (\forall k \in \mathbb{R})$. As shown in the Appendix, a consequence of this symmetry is that for every zero mode at complex number z , where $z = e^{ik}$, there is also a zero mode at z^{-1} .

The simplest lattice with a non-trivial topological polarization, the one-dimensional chain of rotors and springs studied in [44], does not show generalized inversion symmetry. Its rigidity matrix is $\mathcal{R}(z) = c_1 - c_2 z$, so that there is a zero mode at $z = c_1/c_2$, but none at $z^{-1} = c_1/c_2$. This means that [as depicted in Fig. 1(a)] the zero mode is localized on either the right or the left interface, depending on whether $|c_1/c_2| > 1$ or < 1 , indicating the presence of a topological polarization. By contrast, Fig. 1(b) shows a lattice with generalized inversion symmetry, which does not have a topological polarization and has equal numbers of zero modes localized on the left and the right interfaces.

The topological invariant that distinguishes lattices in this classification scheme is calculated from the Singular Value Decomposition (SVD, a generalization of the eigenvalue decomposition) of the rigidity matrix. In SVD, the Fourier-transformed rigidity matrix $\mathcal{R}(k)$ is written as $\mathcal{R} = \mathcal{U} \Lambda_R \mathcal{V}^\dagger$, with \mathcal{U}, \mathcal{V} unitary and Λ_R a rectangular matrix with only real so-called *singular values* along the diagonal. For lattices in which the degrees of freedom and the number of constraints are matched, $\mathcal{R}(k)$ can be transformed into its SVD-flattened version $\mathcal{Q}(k)$ by replacing every nonzero element of Λ_R by 1, yielding a unitary matrix. In the basis in which $\mathcal{R}(k)$ is real, $\mathcal{Q}(k)$ is an orthogonal matrix, equivalent to a rotation matrix, which can be classified into topologically distinct classes. For a hyperstatic lattice in which the number of constraints per unit cell exceeds the number of degrees of freedom per unit cell by one, the number of rows of $\mathcal{Q}(k)$ must exceed its number of columns by 1. Adding a column that is orthogonal to all its column vectors transforms $\mathcal{Q}(k)$ to an orthogonal matrix, which can be classified into topologically distinct classes as described below.

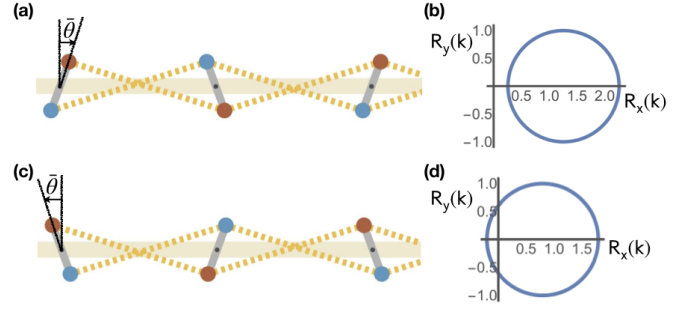


FIG. 2. (Color) Hyperstatic 1D rotor chain with generalized inversion symmetry. (a) Right-leaning rotor chain, where the rotor angle θ is positive (measured from the red rotor head). (b) The winding number (around the origin) in k -space of the rigidity matrix for the right-leaning rotor chain is 0. (c) Left-leaning rotor chain, for which θ is negative. (d) The winding number in k -space of the rigidity matrix for the left-leaning rotor chain is 1.

For an isostatic lattice with generalized inversion symmetry and 2 sites per unit cell, the SVD-flattened rigidity matrix $\mathcal{Q}(k)$ is equivalent to a two-dimensional rotation matrix. The topological invariant classifying such a lattice is the integer winding number of its rotation angle around the unit circle, as the wavenumber k goes from 0 to 2π across the Brillouin zone. In particular, the winding number for the rigidity matrix $R(\lambda, k)$ given by

$$R(\lambda, k) = \begin{pmatrix} (1 - \lambda) - \lambda \cos(k) & -\lambda \sin(k) \\ +\lambda \sin(k) & (1 - \lambda) - \lambda \cos(k) \end{pmatrix} \quad (1)$$

is 0 or 1, depending on whether λ is less than or greater than 0.5. Though $R(\lambda, k)$ is complex in real space, it can be transformed to a rigidity matrix $\tilde{R}(\lambda, k) = U \cdot R(\lambda, k) \cdot U^\dagger$ which is real in real space, where the unitary matrix $U = \frac{1}{2} \begin{pmatrix} 1 + i & -1 - i \\ 1 - i & 1 - i \end{pmatrix}$. Rewriting the above rigidity matrix as a function of $z = e^{ik}$, we find that its determinant vanishes for $z, z^{-1} = \lambda/(1 - \lambda)$, implying the existence of zero modes at both the left and the right interfaces. As λ crosses 0.5, the zero modes interchange between the two interfaces, implying that an interface between two lattices with $\lambda < 0.5$ and $\lambda > 0.5$ is guaranteed to possess localized zero modes, as shown in Fig. 1(b) and described in detail in the Appendix.

Similarly, for an isostatic lattice with generalized inversion symmetry and $N = 3$ sites per unit cell, the SVD-flattened rigidity matrix $\mathcal{Q}(k)$ is equivalent to a three-dimensional rotation matrix. Calculating its topological invariant requires representing $\mathcal{Q}(k)$ by a point in a solid sphere of radius π whose antipodal points are identified, where the radius vector of the point encodes the rotation angle in its magnitude and the rotation axis in its direction. The topological invariant is 0 or 1 depending on whether the loop traced out by $\mathcal{Q}(k)$ (as the wavenumber k goes from 0 to 2π) is contractible or not. All Maxwell lattices obeying generalized inversion symmetry with more than 3 sites per unit cell are similarly

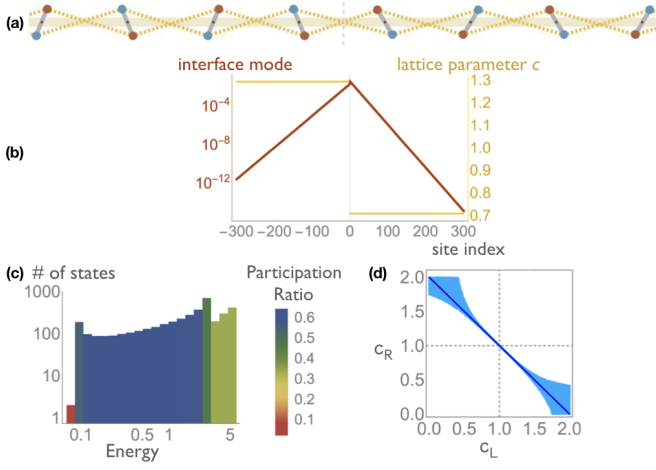


FIG. 3. (Color) Topologically protected localized soft modes at a sharp interface in a hyperstatic lattice with generalized inversion symmetry. (a) A sharp interface between right and left-leaning hyperstatic rotor chains. (b) The localized soft mode (red) at the interface where the lattice parameter c (yellow) changes abruptly. (c) Density of states for this lattice with periodic boundary conditions, showing two topologically protected localized soft modes, one at each interface. (d) The region of parameter space (light blue) for localized soft modes to exist at a sharp interface between a lattice with $c = c_L$ on the left, and $c = c_R$ on the right, and the line $c_L + c_R = 2$ in deep blue.

characterized by a \mathbb{Z}_2 topological invariant [52]. As we demonstrate analytically in the Appendix, a topologically protected gap mode appears at an interface over which this topological invariant changes.

Topological soft modes in a hyperstatic lattice—The study of topological soft modes has hitherto been almost exclusively in the realm of Maxwell lattices. We show that even hyperstatic lattices can have topologically protected mechanical modes in the presence of generalized inversion symmetry. We focus on hyperstatic lattices with one degree of freedom and two constraints per unit cell. For these lattices, the topological invariant has a simple interpretation as the winding number around the origin of the real two-component vector $\vec{R}(k)$ as k crosses the Brillouin zone. Consider a hyperstatic lattice obeying generalized inversion symmetry with the following Fourier transformed rigidity matrix: $\mathcal{R}(k) = (c - \cos k, \sin k)^T$. Its winding number is 1 or 0 for $c < 1$ and $c > 1$ respectively. When c crosses 1, the loop traced out by $\vec{R}(k)$ passes through the origin of the 2D plane, indicating that the lattice must have a bulk zero mode as it crosses over from one topological phase to the other.

For a physical realization of the above rigidity matrix $\mathcal{R}(k)$, it can be transformed to an equivalent rigidity matrix $\tilde{\mathcal{R}}(k)$ that is real in real space:

$$\tilde{\mathcal{R}}(k) = \frac{1}{\sqrt{2}} \begin{pmatrix} 1 & -i \\ 1 & i \end{pmatrix} \cdot \mathcal{R}(k) = \frac{1}{\sqrt{2}} \begin{pmatrix} c - e^{ik} \\ c - e^{-ik} \end{pmatrix}. \quad (2)$$

The rigidity matrix $\tilde{\mathcal{R}}(k)$ can be realized by the hyperstatic rotor chain shown in Figs. 2(a,c) where $c = (a + 2r \sin \theta)/(a - 2r \sin \theta)$, with a being the lattice spacing, r being the distance between the fixed point and the rotor head, and θ being the rotor angle measured from the vertical.

The rotor chains shown in Figs. 2(a,c) belong to topologically distinct classes corresponding to $c > 1$ ($\Leftrightarrow \theta > 0$) and $c < 1$ ($\Leftrightarrow \theta < 0$), with winding numbers 0 and 1, respectively, as shown in Fig. 2(b,d). Allowing the parameter c to vary spatially ($c \rightarrow c_n$) yields the equation of motion (see Appendix for details):

$$\ddot{u}_n = -(c_n - 1)^2 u_n + c_n (u_{n+1} - 2u_n + u_{n-1}) + \frac{c_{n+1} - c_n}{2} u_{n+1} - \frac{c_n - c_{n-1}}{2} u_{n-1}. \quad (3)$$

We now analytically and numerically demonstrate the existence of a topologically protected soft mode localized at the interface. This soft mode is reminiscent of the zero mode that the lattice must pass through as it is continuously deformed from the topological phase on one side of the interface to the topological phase on the other side of the interface. This mode lies in the gap, but not necessarily at low frequencies. We focus on the case in which the stiffness $(c_n - 1)^2$ is small and the gapped mode is soft.

Sharp interface—At a sharp interface between topologically distinct phases of the hyperstatic rotor chain, the parameter c jumps from below 1 to above 1 or vice-versa. Using normal modes of the generalized Bloch form $u_n(t) = u_0 z^n e^{i\omega t}$, we find exact solutions to Eq. (3) for this case, as shown in the Appendix. The existence of this topological mode in the gap is only guaranteed when the gap frequencies coincide on both sides of the interface, as is the case for topological modes generated by conventional Hermitian operators. In our case, this condition is met when the coefficient c_L on the left and c_R on the right satisfy $(c_L - 1)^2 = (c_R - 1)^2$, so that a non-trivial interface has $c_L + c_R = 2$. Taking $c_L = 1 - m_0$ and $c_R = 1 + m_0$, the analytical solution of Eq. (3) for the localized mode has energy $\omega^2 = m_0^2 - m_0^4/(4 - m_0^2)$, and decay rates on the left and right sides of the interface $z_L = (2 - m_0)/((2 + m_0)(1 - m_0))$ and $z_R = (1 + m_0)(2 - m_0)/(2 + m_0)$, respectively.

To confirm our analytical predictions about the soft modes localized at a sharp interface, we numerically study a hyperstatic chain of $N = 4000$ rotors with periodic boundary conditions, and sharp interfaces at $n = 1000$ and $n = 3000$, where the lattice parameter c_n jumps from 0.7 to 1.3 and back to 0.7. One of the sharp interfaces is shown in Fig. 3(a) and the topological interface mode is plotted in Fig. 3(b), in red, along with the parameter c_n (yellow). The density of states

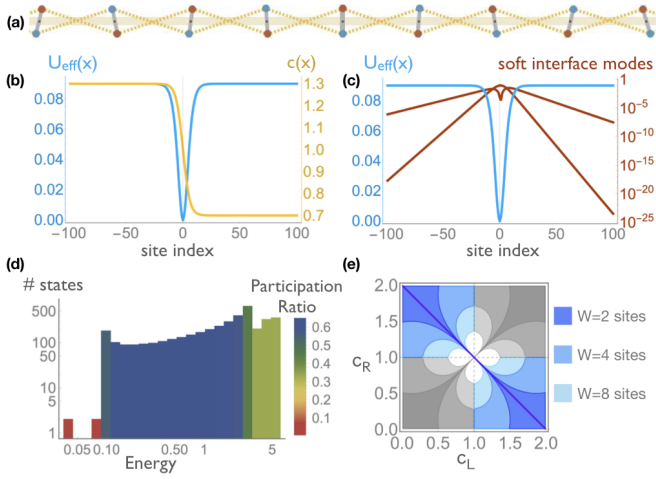


FIG. 4. (Color) Topologically protected localized soft modes at a smooth interface in a hyperstatic lattice with generalized inversion symmetry. (a) A smooth interface between right and left-leaning hyperstatic rotor chains. (b) For smoothly varying parameter c , the localized interface modes can be mapped to bound states in an effective potential (blue) for the Schrödinger equation. (c) The two lowest localized soft modes (red) at the interface where the lattice parameter c (yellow) changes smoothly. (d) Density of states for this lattice with periodic boundary conditions, showing two topologically protected modes at each interface. (e) The region of parameter space (blue) in which localized soft modes exist at a smooth topological interface with $c = c_L$ on the left, and $c = c_R$ on the right, calculated in the continuum approximation (see Ref. [54] and Eq. (C21) in the Appendix) for different interface widths W . The line $c_L + c_R = 2$ is shown in deep blue. The grey regions correspond to the non-topological interface, when localized interface modes are not guaranteed to exist.

shown in Fig. 3(c) reveals two soft modes localized at the two interfaces, having the lowest energy and lowest participation ratio. The analytically derived values for the localized mode energy and the mode decay rates are found to agree with the numerical calculations shown in Figs. 3(b,c). As shown in Fig. 3(d), as the difference between the two regions increases the gapped mode persists even when the constraint $c_L + c_R = 2$ is violated.

Smooth interface—To study the modes localized at a smooth interface between the two topologically distinct phases of the hyperstatic rotor chain, we take the continuum limit of Eq. (3) with $c_n \rightarrow c(x) = 1 + m(x)$ and $u_n(t) \rightarrow u(x, t)$, $u(x, t) = u(x) e^{i\omega t}$ to get

$$(\omega^2 - m^2)u + (1 + m)u'' + m'u' = 0, \quad (4)$$

with u' etc. denoting spatial derivatives.

In the limit $m(x) \ll 1$, i.e., in the region where $c(x)$ is close to 1, the above equation of motion becomes: $u''(x) + (\omega^2 - m^2)u = 0$, bearing a close resemblance to the time-independent Schrödinger equation with $2m/\hbar^2 = 1$, the energy $E = \omega^2$, and the potential $U(x) = m^2(x)$.

In this analogy, a smooth interface corresponds to a potential well with a minimum energy of $U(x) = 0$ when $m(x) = 0$, $c(x) = 1$, and depth given by the asymptotic values of $m^2(x)$ on either side of the well. When the asymptotic values of $m^2(x)$ on the two sides of the interface are equal, i.e., the potential $U(x)$ is symmetric about its minimum, at least one bound state solution exists irrespective of the depth of the potential well [54]. This guarantees the existence of at least one soft localized mode at the interface.

An analytical solution for the localized mode is made possible by the analogy with the Schrödinger equation, for which the solution is known for $m(x) = m_0 \tanh(x/W)$ [55]. To confirm our analytical calculations, we numerically study a hyperstatic chain of $N = 4000$ rotors with periodic boundary conditions, with $m_0 = 0.3$, $w = 6$, and smooth interfaces for which $m(x) = m_0 \tanh(x/W)$ as shown in Fig. 4. Two localized soft modes at one of the interfaces are shown in Fig. 4(c) with the modes in red and the effective potential $U(x)$ in blue. The density of states shown in Fig. 4(d) confirms two soft modes localized at each interface, having the lowest energies and lowest participation ratios, shown in red. Our numerical calculations of the mode decay rate and the mode energies shown in Figs. 4(c,d) are in agreement with the analytical solution described in the Appendix.

In Fig. 4(e), we plot the region of parameter space $\{c_L, c_R\}$ for which a soft mode is localized at the interface. This region is calculated using the criterion for a bound state to exist in an asymmetric potential well [54] (see Appendix). The gapped mode is found to persist even when the constraint $c_L + c_R = 2$ is violated, with larger interface widths allowing for greater deviations from the constraint.

Conclusions—The theoretical models that we have presented rely on generalized inversion symmetry to define topological invariants and create robust soft modes at interfaces. However, even if this symmetry is weakly broken, these soft modes in rigid materials persist over a region of design space, as illustrated in our numerical calculations. These symmetry-protected soft modes can be achieved in materials which are created to be stable, and therefore overconstrained, and whose symmetries will be necessarily broken by thermal or manufacturing disorder. This suggests a pathway towards miniaturizing topological mechanical materials from metamaterials at the macroscale to structured matter self-assembled from polymeric, colloidal, or molecular constituents at the microscale. Designing topologically protected soft modes in these materials may lead to future applications from cushioning using soft regions [48] to controlled failure at topological interfaces [18].

Acknowledgments—A.S. acknowledges the support of the Engineering and Physical Sciences Research Council (EPSRC) through New Investigator Award No. EP/T000961/1. H.K. thanks Jeremy England for his support.

-
- [1] S. D. Huber, *Nature Physics* **12**, 621 (2016).
 - [2] K. Bertoldi, V. Vitelli, J. Christensen, and M. Van Hecke, *Nature Reviews Materials* **2**, 1 (2017).
 - [3] X. Mao and T. C. Lubensky, *Annual Review of Condensed Matter Physics* **9**, 413 (2018).
 - [4] L. Lu, J. D. Joannopoulos, and M. Soljačić, *Nature Photonics* **8**, 821 (2014).
 - [5] T. Ozawa *et al.*, *Reviews of Modern Physics* **91**, 015006 (2019).
 - [6] Yuto, Z. Gong, and M. Ueda, *Non-hermitian physics*, 2020, arXiv:2006.01837.
 - [7] M. Z. Hasan and C. L. Kane, *Reviews of modern physics* **82**, 3045 (2010).
 - [8] K. von Klitzing, *Rev. Mod. Phys.* **58**, 519 (1986).
 - [9] D. J. Thouless, M. Kohmoto, M. P. Nightingale, and M. den Nijs, *Phys. Rev. Lett.* **49**, 405 (1982).
 - [10] F. D. M. Haldane, *Phys. Rev. Lett.* **61**, 2015 (1988).
 - [11] J. M. Kosterlitz and D. J. Thouless, *J. Phys. C: Solid State Phys.* **6**, 1181 (1973).
 - [12] M. C. Rechtsman *et al.*, *Nature* **496**, 196 (2013).
 - [13] L. M. Nash *et al.*, *PNAS* **112**, 14495 (2015).
 - [14] P. Wang, L. Lu, and K. Bertoldi, *Phys. Rev. Lett.* **115**, 104302 (2015).
 - [15] V. Peano, C. Brendel, M. Schmidt, and F. Marquardt, *Phys. Rev. X* **5**, 031011 (2015).
 - [16] R. Süssstrunk and S. D. Huber, *Science* **349**, 47 (2015).
 - [17] A. B. Khanikaev, R. Fleury, S. H. Mousavi, and A. Alù, *Nat Commun* **6**, 1 (2015).
 - [18] J. Paulose, A. S. Meeussen, and V. Vitelli, *Proceedings of the National Academy of Sciences* **112**, 7639 (2015).
 - [19] C. He *et al.*, *Nature Physics* **12**, 1124 (2016).
 - [20] Z.-G. Chen and Y. Wu, *Phys. Rev. Applied* **5**, 054021 (2016).
 - [21] Bryan Gin-ge Chen and B. Liu and A. A. Evans and J. Paulose and I. Cohen and V. Vitelli and C.D. Santangelo, *Physical review letters* **116**, 135501 (2016).
 - [22] A. Souslov, B. C. van Zuiden, D. Bartolo, and V. Vitelli, *Nature Physics* **13**, 1091 (2017).
 - [23] A. Murugan and S. Vaikuntanathan, *Nat Commun* **8**, 1 (2017).
 - [24] K. Dasbiswas, K. K. Mandadapu, and S. Vaikuntanathan, *PNAS* **115**, E9031 (2018).
 - [25] J. Vila, R. K. Pal, and M. Ruzzene, *Phys. Rev. B* **96**, 134307 (2017).
 - [26] G. Trainiti, J. J. Rimoli, and M. Ruzzene, *Journal of Applied Physics* **123**, 091706 (2017).
 - [27] N. P. Mitchell, L. M. Nash, D. Hexner, A. M. Turner, and W. T. M. Irvine, *Nature Phys* **14**, 380 (2018).
 - [28] A. Souslov, K. Dasbiswas, M. Fruchart, S. Vaikuntanathan, and V. Vitelli, *Physical review letters* **122**, 128001 (2019).
 - [29] R. Süssstrunk and S. D. Huber, *PNAS* **113**, E4767 (2016).
 - [30] S. Ryu, A. P. Schnyder, A. Furusaki, and A. W. W. Ludwig, *New J. Phys.* **12**, 065010 (2010).
 - [31] S. Yao and Z. Wang, *Phys. Rev. Lett.* **121**, 086803 (2018), Publisher: American Physical Society.
 - [32] K. Esaki, M. Sato, K. Hasebe, and M. Kohmoto, *Phys. Rev. B* **84**, 205128 (2011).
 - [33] S.-D. Liang and G.-Y. Huang, *Phys. Rev. A* **87**, 012118 (2013).
 - [34] T. E. Lee, *Phys. Rev. Lett.* **116**, 133903 (2016).
 - [35] D. Leykam, K. Y. Bliokh, C. Huang, Y.-D. Chong, and F. Nori, *Phys. Rev. Lett.* **118**, 040401 (2017).
 - [36] H. Menke and M. M. Hirschmann, *Phys. Rev. B* **95**, 174506 (2017).
 - [37] Y. Xu, S.-T. Wang, and L.-M. Duan, *Phys. Rev. Lett.* **118**, 045701 (2017).
 - [38] J. González and R. A. Molina, *Phys. Rev. B* **96**, 045437 (2017).
 - [39] Y. Xiong, *J. Phys. Commun.* **2**, 035043 (2018).
 - [40] H. Shen, B. Zhen, and L. Fu, *Phys. Rev. Lett.* **120**, 146402 (2018).
 - [41] W. Hu, H. Wang, P. P. Shum, and Y. D. Chong, *Phys. Rev. B* **95**, 184306 (2017).
 - [42] K. Kawabata, K. Shiozaki, M. Ueda, and M. Sato, *Physical Review X* **9**, 041015 (2019).
 - [43] C. Scheibner, W. T. M. Irvine, and V. Vitelli, *Non-hermitian band topology and skin modes in active elastic media*, 2020, arXiv:2001.04969.
 - [44] C. L. Kane and T. C. Lubensky, *Nature Physics* **10**, 39 (2014).
 - [45] B. G.-g. Chen, N. Upadhyaya, and V. Vitelli, *Proceedings of the National Academy of Sciences* **111**, 13004 (2014).
 - [46] D. Z. Rocklin, Bryan Gin-ge Chen, M. Falk, V. Vitelli, and T. Lubensky, *Physical review letters* **116**, 135503 (2016).
 - [47] J. Paulose, Bryan Gin-ge Chen, and V. Vitelli, *Nature Physics* **11**, 153 (2015).
 - [48] O. R. Bilal, R. Süssstrunk, C. Daraio, and S. D. Huber, *Advanced Materials* **29**, 1700540 (2017).
 - [49] G. Baardink, A. Souslov, J. Paulose, and V. Vitelli, *Proceedings of the National Academy of Sciences* **115**, 489 (2018).
 - [50] S. Guest and J. Hutchinson, *Journal of the Mechanics and Physics of Solids* **51**, 383 (2003).
 - [51] A. Saremi and Z. Rocklin, *Phys. Rev. B* **98**, 180102(R) (2018).
 - [52] K. Roychowdhury and M. J. Lawler, *Phys. Rev. B* **98**, 094432 (2018).
 - [53] T. Lubensky, C. Kane, X. Mao, A. Souslov, and K. Sun, *Reports on Progress in Physics* **78**, 073901 (2015).
 - [54] C. A. Kocher, *American Journal of Physics* **45**, 71 (1977).
 - [55] L. D. Landau and E. M. Lifshitz, *Quantum Mechanics: Non-Relativistic Theory* (Elsevier, 1981).

Appendix A: Generalized Inversion symmetry

Generalized inversion symmetry in a d -dimensional mechanical lattice requires (i) that there exist a basis in which the Fourier-transformed rigidity matrix $\mathcal{R}(k)$ is real for real wavenumber k and (ii) that the rigidity matrix in real space be real, as must be the case for a physically realizable rigidity matrix. Written in terms of the complex wavenumber $z = e^{ik}$, the rigidity matrix then takes the form $\mathcal{R}(z) = \sum_n U^\dagger \cdot R_n z^n \cdot W$, where substituting $z = e^{ik}$ gives the

Fourier-transformed rigidity matrix $\mathcal{R}(k) = \mathcal{R}(z)|_{z=e^{ik}}$. Here, U, W are unitary matrices such that $U \cdot \mathcal{R}(k) \cdot W^\dagger$ is real, hence satisfying condition (i). This requires that $R_n = R_n^*$, where R_n^* is the complex conjugate of R_n . For a zero mode \mathbf{u} at $z = z_0$,

$$\begin{aligned} \mathcal{R}(z_0) \cdot \mathbf{u} = 0 &\Rightarrow \sum_n U^\dagger \cdot R_n z_0^n \cdot W \cdot \mathbf{u} = 0 \Rightarrow \sum_n R_n z_0^n \cdot W \cdot \mathbf{u} = 0 \Rightarrow \sum_n R_n^* (z_0^*)^n \cdot W^* \cdot \mathbf{u}^* = 0 \\ &\Rightarrow \sum_n R_{-n} (z_0^*)^n \cdot W^* \cdot \mathbf{u}^* = 0 \Rightarrow \sum_n R_n (z_0^*)^{-n} \cdot W^* \cdot \mathbf{u}^* = 0 \Rightarrow \sum_n R_n [(z_0^*)^{-1}]^n \cdot W^* \cdot \mathbf{u}^* = 0 \\ &\Rightarrow \sum_n \left(U \cdot \mathcal{R}(z_0^{*-1}) \cdot W^\dagger \right) \cdot W^* \cdot \mathbf{u}^* = 0 \Rightarrow \sum_n \mathcal{R}(z_0^{*-1}) \cdot (W^\dagger \cdot W^* \cdot \mathbf{u}^*) = 0 \end{aligned} \quad (\text{A1})$$

Hence, condition (i) implies that for every zero mode \mathbf{u} at $z = z_0$ there is a zero mode $W^\dagger \cdot W^* \cdot \mathbf{u}^*$ at $z = (z_0^*)^{-1}$. Additionally, condition (ii) requires that $U^\dagger \cdot R_n \cdot W \in \mathbb{R}, \forall n$. For a zero mode \mathbf{u} at $z = z_0$,

$$\begin{aligned} \mathcal{R}(z_0) \cdot \mathbf{u} = 0 &\Rightarrow \sum_n U^\dagger \cdot R_n z_0^n \cdot W \cdot \mathbf{u} = 0 \Rightarrow \sum_n (z_0^*)^n (U^T \cdot R_n^* \cdot W^*) \cdot \mathbf{u}^* = 0 \\ &\Rightarrow \sum_n (z_0^*)^n (U^\dagger \cdot R_n \cdot W) \cdot \mathbf{u}^* = 0 \Rightarrow \mathcal{R}(z_0^*) \cdot \mathbf{u}^* = 0 \end{aligned} \quad (\text{A2})$$

Hence, condition (ii) implies that for every zero mode \mathbf{u} at $z = z_0$ there is a zero mode \mathbf{u}^* at $z = z_0^*$. Since generalized inversion symmetry requires both conditions (i) and (ii) be satisfied, a zero mode \mathbf{u} at $z = z_0$ will always be accompanied by a zero mode \mathbf{u}^* at z_0^* , a zero mode $W^\dagger \cdot W^* \cdot \mathbf{u}^*$ at $z = (z_0^*)^{-1}$, and as a consequence of the above, a zero mode $W^T \cdot W \cdot \mathbf{u}$ at $z = z_0^{-1}$.

Mechanical lattices with generalized inversion symmetry can be classified according to the homotopy groups of their Fourier-transformed rigidity matrix, as in [52]. Any matrix, and hence any rigidity matrix $\mathcal{R}(k)$, has a singular value decomposition: $\mathcal{R} = \mathcal{U} \cdot \Lambda_R \cdot \mathcal{V}^\dagger$, and can be continuously transformed into its SVD flattened version $\mathcal{Q} = \mathcal{U} \cdot \tilde{\Lambda}_R \cdot \mathcal{V}^\dagger$ where \mathcal{U}, \mathcal{V} are unitary matrices, and $\tilde{\Lambda}_R$ is obtained by replacing every element of Λ_R by 1 or 0 according to whether its magnitude is non-vanishing or vanishing. The SVD-flattened matrix $\mathcal{Q}(k)$ has the same dimensions as $\mathcal{R}(k)$, and encodes the topological properties of $\mathcal{R}(k)$.

In the classification, Maxwell lattices which do not obey generalized inversion symmetry have unitary SVD flattened rigidity matrices, which have a non-trivial fundamental group $\pi_1[U(N)] = \mathbb{Z}$, where the winding number defined by Kane and Lubensky is the integer topological invariant characterizing the different homotopy classes. Maxwell lattices obeying generalized inversion symmetry have orthogonal rigidity matrices with a non-trivial fundamental group $\pi_1[O(N)]$ depending on N , which is the dimension of the rigidity matrix in Fourier space, which is the number of sites per unit cell. This classification gives a non-trivial fundamental group for non-Maxwell lattices with ‘realness’ symmetry in which the the number of degrees of freedom and number of constraints per unit cell are mismatched by $|\nu| = 1$, opening up the possibility of topologically protected modes in non-Maxwell lattices.

In the rest of the Appendix, we show in detail how topologically protected modes arise at interfaces between topologically distinct lattices with generalized inversion symmetry, for the case of one-dimensional Maxwell lattices with $N = 2, 3$ sites per unit cell, and for a one-dimensional hyperstatic lattice with 2 constraints and 1 degree of freedom per unit cell.

Appendix B: Maxwell Lattices with generalized inversion symmetry

Maxwell lattices with generalized inversion symmetry have rigidity matrices whose SVD flattened versions that belong to the group of orthogonal matrices $O(N)$. Their fundamental homotopy group: $\pi_1[O(N)]$ is trivial for $N = 1$, \mathbb{Z} for $N = 2$, and \mathbb{Z}_2 for $N \geq 3$, where N is the number of sites per unit cell.

In this section, we study Maxwell lattices with generalized inversion symmetry belonging to different homotopy classes for $N = 2$ and $N = 3$, which displays the generic $N > 2$ homotopy class, define topological invariants that distinguish these lattices, and show the presence of topologically protected zero modes at interfaces between lattices belonging to different homotopy classes.

1. Two sites per unit cell

In this case, the SVD-flattened rigidity matrix $\mathcal{Q}(k)$ is a 2×2 orthogonal matrix, with determinant ± 1 . Multiplying $\mathcal{Q}(k)$ by its determinant gives an $SO(2)$ matrix, which can be classified by the number of times its rotation angle

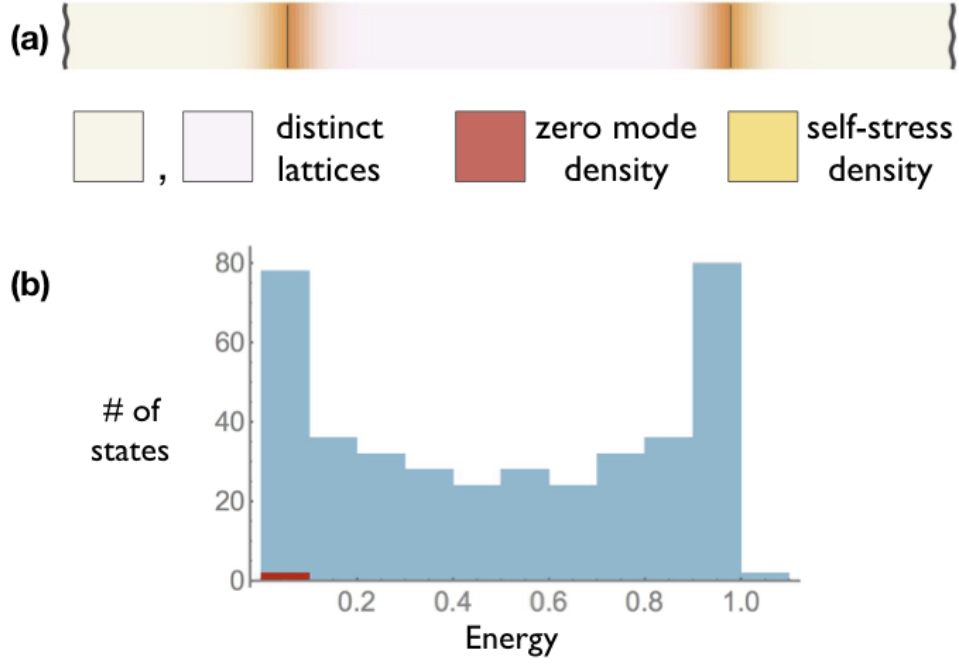


FIG. 5. Schematic of a material based on a Maxwell lattice with 2 sites per unit cell, obeying generalized inversion symmetry. The material with the rigidity matrix $\tilde{R}(\lambda, k)$ in Eq. (B2), where $\lambda = 0.55$ in the middle region shown in light purple, and $\lambda = 0.45$ for the left and right regions shown in light beige. (a) In the presence of generalized inversion symmetry, Maxwell lattices have no topological polarization and consequently have zero modes and self-stress states localized on the both interfaces. (b) The density of states for this system, with the zero modes shown in red.

winds around the unit circle, as the wavenumber k goes from 0 to 2π . The winding number of the rotation angle of the SVD flattened rigidity matrix gives an integer topological invariant distinguishing lattices belonging to different homotopy classes. Since the one-dimensional Brillouin Zone and the rotation angle of a rotation in two dimensions are both defined modulo 2π , they are both topologically equivalent to a circle, S^1 , and this homotopy class corresponds to a map of S^1 to itself.

An example of such a rigidity matrix is:

$$R(\lambda, k) = -\lambda R(k) + (1 - \lambda) I = \begin{pmatrix} (1 - \lambda) - \lambda \cos(k) & -\lambda \sin(k) \\ +\lambda \sin(k) & (1 - \lambda) - \lambda \cos(k) \end{pmatrix} \quad (B1)$$

where $R(k)$ is a 2×2 rotation matrix with rotation angle k . The winding number of the rotation angle of $R(\lambda, k)$ is 0 or 1, depending on whether λ is less than or greater than 0.5.

The above rigidity matrix is real in momentum space, and thus necessarily complex in real space. However, it can be transformed to a rigidity matrix which is real in real space via the following unitary transformation:

$$\begin{aligned} \tilde{R}(\lambda, k) &= U \cdot R(\lambda, k) \cdot U^\dagger, \quad U = \frac{1}{2} \begin{pmatrix} 1 + i & -1 - i \\ 1 - i & 1 - i \end{pmatrix} \\ \Rightarrow \tilde{R}(\lambda, k) &= \begin{pmatrix} (1 - \lambda) - \lambda \cos(k) & -i \lambda \sin(k) \\ -i \lambda \sin(k) & (1 - \lambda) - \lambda \cos(k) \end{pmatrix} \end{aligned} \quad (B2)$$

To further simplify our analysis, the above rigidity matrix is diagonalized via the following orthogonal transformation:

$$\begin{aligned} R'(\lambda, k) &= O \cdot \tilde{R}(\lambda, k) \cdot O^T, \quad O = \frac{1}{\sqrt{2}} \begin{pmatrix} 1 & 1 \\ -1 & 1 \end{pmatrix} \\ \Rightarrow R'(\lambda, k) &= \begin{pmatrix} (1 - \lambda) - \lambda e^{ik} & 0 \\ 0 & (1 - \lambda) - \lambda e^{-ik} \end{pmatrix} \end{aligned} \quad (B3)$$

To study the localized zero modes at an interface between lattices belonging to distinct homotopy classes, we rewrite the above rigidity matrix as a function of the complex number $z = e^{ik}$:

$$R'(\lambda, z) = \begin{pmatrix} (1 - \lambda) - \lambda z & 0 \\ 0 & (1 - \lambda) - \lambda z^{-1} \end{pmatrix} \quad (B4)$$

The determinant of the above rigidity matrix vanishes at $z(\lambda) = \{-\frac{\lambda}{1-\lambda}, -\frac{1-\lambda}{\lambda}\}$. Notice that the two values of z , are of the form $z = z_0, z_0^{-1}$, a pair since $z(\lambda)$ is real, as expected for lattices obeying generalized inversion symmetry.

This implies that there are left-growing ($|z(\lambda)| < 1$) and right-growing ($|z(\lambda)| > 1$) zero modes. The zero modes are orthogonal to each other and are in fact a natural basis for the transformed matrix: $\{(1, 0), (0, 1)\}$. As λ crosses 0.5, the winding number of the rotation angle of the matrix changes from $0 \rightarrow 1$, and the zero modes change from $\{\text{right growing}, \text{left growing}\}$ to $\{\text{left growing}, \text{right growing}\}$.

This implies that an interface between two lattices with $\lambda < 0.5$ and $\lambda > 0.5$, would have localized zero modes which would grow at the rates predicted by $z(\lambda)$ on either side of the interface. We have confirmed this observation numerically, by explicitly calculating the zero modes of the dynamical matrix $D = R^T \cdot R$, where R is the real space version of the rigidity matrix in Eq. (B2) for a one-dimensional periodic system with the two topologically distinct phases $\lambda > 0.5, \lambda < 0.5$ spanning 2000 unit cells each.

Such a real-space matrix may be readily obtained from the previous forms. If a term $cz^n = c \exp(ikn)$ appears in an element of the rigidity matrix it simply corresponds to the same factor c connecting a degree of freedom in any cell indexed n' to one in the cell $n' + n$.

2. Three sites per unit cell

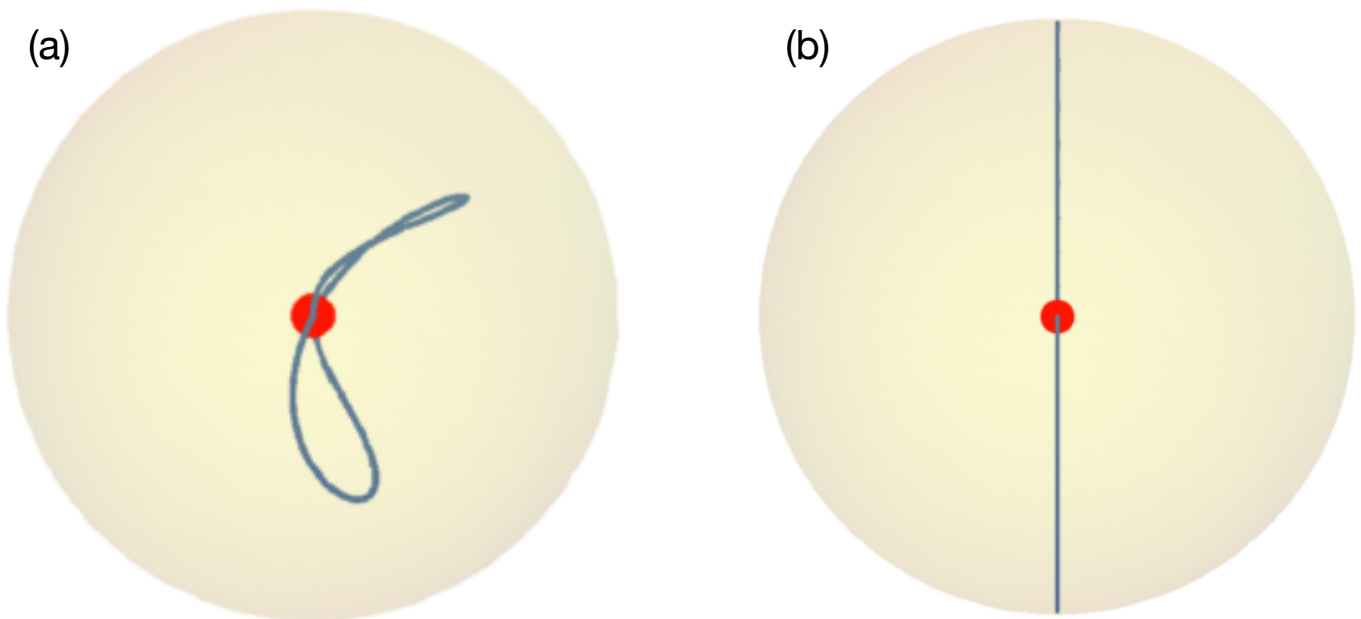


FIG. 6. (a) a closed loop on the $SO(3)$ sphere which can be continuously shrunk to a point (b) a closed loop on the $SO(3)$ sphere which can not be shrunk to a point, since it closes through antipodal points.

In this case, the SVD-flattened rigidity matrix $\mathcal{Q}(k)$ is a 3×3 orthogonal matrix, with determinant ± 1 . Multiplying $\mathcal{Q}(k)$ by its determinant gives an $SO(3)$ matrix for each k . Any $SO(3)$ matrix can be represented by a point in a solid sphere (or “ball”) of radius π whose radius vector is along the rotation axis of the matrix, and whose distance from the center of sphere is given by the rotation angle of the matrix [52]. Antipodal points on the surface of this solid sphere are identical since a rotation angle of π along an axis is the same as a rotation angle of $-\pi$ along the opposite axis. As k varies from 0 to 2π , the path traced out by the SVD-flattened matrix $\mathcal{Q}(k) \in SO(3)$ could either be a closed loop which can be shrunk to a point as in Fig. 6(a), or a closed loop which can not be shrunk to a point as in Fig. 6(b) since it closes by piercing the surface of the sphere and coming out through the opposite side. However, a path can be continuously transformed such that pairs of surface crossings cancel out, so that any paths with the same parity of surface crossings are equivalent. Hence the two different homotopy classes of 3×3 rigidity matrices with generalized inversion symmetry are distinguished by a \mathbb{Z}_2 topological invariant: the number of times modulo 2 that the path traced out by the SVD-flattened matrix pierces the surface of the $SO(3)$ sphere where antipodal points are identified.

An example of a topologically non-trivial 3×3 rigidity matrix, inspired by the 2×2 rigidity matrix in the previous

section, is:

$$R(\lambda, k) = -\lambda R_z(k) + (1 - \lambda) I = \begin{pmatrix} (1 - \lambda) - \lambda \cos(k) & \lambda \sin(k) & 0 \\ -\lambda \sin(k) & (1 - \lambda) - \lambda \cos(k) & 0 \\ 0 & 0 & 1 \end{pmatrix} \quad (\text{B5})$$

where $R_z(k)$ is a 3×3 rotation matrix with rotation angle k about the z-axis. The number of times that the path traced out by $R(\lambda, k)$ pierces the $SO(3)$ sphere is 0 or 1, depending on whether λ is less than or greater than 0.5, as shown in Fig. 6.

Although, we can write the following more general form for a real rigidity matrix:

$$R(\lambda, k) = O(k) \cdot \begin{pmatrix} (1 - \lambda) + \lambda \cos(k) & -\lambda \sin(k) & 0 \\ \lambda \sin(k) & (1 - \lambda) + \lambda \cos(k) & 0 \\ 0 & 0 & 1 \end{pmatrix} \cdot O^T(k); O(k) = R_z(\alpha(k)) \cdot R_y(\beta(k)) \cdot R_x(\gamma(k)) \quad (\text{B6})$$

$$\text{where } 0 \leq \alpha(k), \beta(k), \gamma(k) \leq \pi/2, \quad \text{and} \quad \alpha(0) = \alpha(\pi) = \beta(0) = \beta(\pi) = \gamma(0) = \gamma(\pi) = 0$$

the path traced out by the above rigidity matrix in the $SO(3)$ sphere can be smoothly transformed to the path traced out by the rigidity matrix given in Eq. (B5), and hence will have the same topological invariant as the rigidity matrix in Eq. (B5). Since the topology of the above more general rigidity matrix is captured by the simpler rigidity matrix given in Eq. (B5), we proceed to study the simpler case.

The rigidity matrix though complex in real space, is easily transformed to a rigidity matrix which is real in real space via the following unitary transformation:

$$\begin{aligned} \tilde{R}(\lambda, k) &= U \cdot R(\lambda, k) \cdot U^\dagger, \quad U = \begin{pmatrix} (1+i)/2 & (-1-i)/2 & 0 \\ (1-i)/2 & (1-i)/2 & 0 \\ 0 & 0 & 1 \end{pmatrix} \\ \Rightarrow \tilde{R}(\lambda, k) &= \begin{pmatrix} (1-\lambda) + \lambda \cos(k) & i \lambda \sin(k) & 0 \\ i \lambda \sin(k) & (1-\lambda) + \lambda \cos(k) & 0 \\ 0 & 0 & 1 \end{pmatrix} \end{aligned} \quad (\text{B7})$$

To further simplify our analysis, we diagonalize the above rigidity matrix via the following orthogonal transformation:

$$\begin{aligned} R'(\lambda, k) &= O \cdot \tilde{R}(\lambda, k) \cdot O^T, \quad O = \begin{pmatrix} 1/\sqrt{2} & 1/\sqrt{2} & 0 \\ -1/\sqrt{2} & 1/\sqrt{2} & 0 \\ 0 & 0 & 1 \end{pmatrix} \\ \Rightarrow R'(\lambda, k) &= \begin{pmatrix} (1-\lambda) + \lambda e^{ik} & 0 & 0 \\ 0 & (1-\lambda) + \lambda e^{-ik} & 0 \\ 0 & 0 & 1 \end{pmatrix} \end{aligned} \quad (\text{B8})$$

To study the localized zero modes at an interface between lattices belonging to distinct homotopy classes, we rewrite the above rigidity matrix as a function of the complex number $z = e^{ik}$:

$$R'(\lambda, z) = \begin{pmatrix} (1-\lambda) + \lambda z & 0 & 0 \\ 0 & (1-\lambda) + \lambda z^{-1} & 0 \\ 0 & 0 & 1 \end{pmatrix} \quad (\text{B9})$$

The determinant of the above rigidity matrix vanishes at $z(\lambda) = \{-\frac{\lambda}{1-\lambda}, -\frac{1-\lambda}{\lambda}\}$, where the product of the two roots is 1, at values of z of the form $z = z_0, z_0^{-1}$, a pair since $z(\lambda)$ is real, as expected for lattices with generalized inversion symmetry. This implies that there is a left growing ($|z(\lambda)| < 1$) and a right growing ($|z(\lambda)| > 1$) zero mode. The zero modes are orthogonal to each other: $\{(1, 0, 0), (0, 1, 0)\}$. As λ crosses 0.5, the number of times the path traced out by the rigidity matrix pierces the $SO(3)$ sphere changes from $0 \rightarrow 1$, and the zero modes change from $\{\text{left growing}, \text{right growing}\}$ to $\{\text{right growing}, \text{left growing}\}$.

This implies that an interface between lattices with $\lambda < 0.5$ and $\lambda > 0.5$ would have localized zero modes which would grow at the rates predicted by $z(\lambda)$ on either side of the interface. This is confirmed numerically.

Appendix C: A hyperstatic lattice with generalized inversion symmetry

For a hyperstatic lattice with generalized inversion symmetry, with 2 springs and 1 degree of freedom per unit cell, there is a choice of basis in which the Fourier transform of the rigidity matrix will be a real 2×1 matrix,

which can be thought of as a real two-vector. The space of 2×1 rigidity matrices can be classified according to the fundamental homotopy group of their SVD flattened versions, giving \mathbb{Z} distinct homotopy classes characterized by a integer topological invariant: the winding number of the two-vector $\tilde{R}(k)$ as k goes from $0 \rightarrow 2\pi$.

An example of such a Fourier transformed rigidity matrix is:

$$R(k) = \begin{pmatrix} c - \cos(k) \\ \sin(k) \end{pmatrix} \quad (C1)$$

The winding number of the above matrix goes from 1 to 0 as $|c|$ goes from $|c| < 1$ to $|c| > 1$. As $|c|$ passes through 1, the bulk energy gap closes, i.e. the lowest energy: $\min_k \{R^\dagger(k)R(k)\} = \min_k \{1 + c^2 - 2c \cos(k)\} = (1 - |c|)^2$ goes to zero at $|c| = 1$, and is positive otherwise.

Since the above rigidity matrix is real in momentum space, it is necessarily complex in real space. However, it can be easily transformed to a rigidity matrix that is real in real space via the following unitary transformation:

$$\begin{aligned} \mathcal{R}(k) &= U \cdot R(k) = \begin{pmatrix} 1 & 0 \\ 0 & i \end{pmatrix} \cdot \begin{pmatrix} c - \cos(k) \\ \sin(k) \end{pmatrix} \\ \Rightarrow \mathcal{R}(k) &= \begin{pmatrix} c - \cos(k) \\ i \sin(k) \end{pmatrix} \end{aligned} \quad (C2)$$

The above matrix can be further simplified via an orthogonal transformation:

$$\begin{aligned} \tilde{R}(k) &= O \cdot \mathcal{R}(k) = \begin{pmatrix} \frac{1}{\sqrt{2}} & \frac{-1}{\sqrt{2}} \\ \frac{1}{\sqrt{2}} & \frac{1}{\sqrt{2}} \end{pmatrix} \cdot \begin{pmatrix} c - \cos(k) \\ i \sin(k) \end{pmatrix} \\ \Rightarrow \tilde{R}(k) &= \frac{1}{\sqrt{2}} \begin{pmatrix} c - e^{ik} \\ c - e^{-ik} \end{pmatrix} \end{aligned} \quad (C3)$$

which can be realized by a chain of rotors connected by springs shown in Fig. 2 of the manuscript, for which the rigidity matrix $\mathcal{R}'(k)$ is:

$$\mathcal{R}'(k) = \frac{a - 2r \sin \theta}{\sqrt{a^2 + 4r^2 \cos^2 \theta}} \begin{pmatrix} \frac{a+2r \sin \theta}{a-2r \sin \theta} - e^{ik} \\ \frac{a+2r \sin \theta}{a-2r \sin \theta} - e^{-ik} \end{pmatrix} \quad (C4)$$

where a is the lattice spacing, r is the distance between the fixed point and the rotor head, and θ is the rotor angle measured from the vertical for the rotor head in red, as shown in Fig. 2(a),(c) of the manuscript. $\tilde{R}(k) \equiv \mathcal{R}'(k)$ up to the multiplication of a scalar, with $c = (a + 2r \sin \theta)/(a - 2r \sin \theta)$.

We now derive the dynamical equation of motion in real space for the rigidity matrix given in Eq. (C3)

The rigidity matrix in real space corresponding to the Fourier transformed matrix given in Eq. C1 is given by:

$$\begin{pmatrix} R_{2j-1,j'} \\ R_{2j,j'} \end{pmatrix} = \frac{1}{\sqrt{2}} \begin{pmatrix} c_j \delta_{j,j'} - \delta_{j,j'+1} \\ c_j \delta_{j,j'} - \delta_{j,j'-1} \end{pmatrix} \quad (C5)$$

The corresponding real space equation of motion is given by:

$$\begin{aligned}
\ddot{\mathbf{u}} &= -\overset{\leftrightarrow}{\mathbf{D}} \cdot \mathbf{u} = -\mathbf{R}^T \cdot \mathbf{R} \cdot \mathbf{u} \\
\Rightarrow \ddot{u}_n &= -\sum_{j,l} R_{n,j}^T R_{j,l} u_l = -\sum_{j,l} R_{j,n} R_{j,l} u_l \\
&= -\sum_{j=1}^N \sum_{l=1}^N (R_{2j-1,n} R_{2j-1,l} + R_{2j,n} R_{2j,l}) u_l \\
&= -\frac{1}{2} \sum_{j=1}^N \sum_{l=1}^N ((c_j \delta_{j,n} - \delta_{j,n+1}) (c_j \delta_{j,l} - \delta_{j,l+1}) + (c_j \delta_{j,n} - \delta_{j,n-1}) (c_j \delta_{j,l} - \delta_{j,l-1})) u_l \\
&= -\sum_{j=1}^N \sum_{l=1}^N \left(c_j^2 \delta_{j,n} \delta_{j,l} + \frac{1}{2} (\delta_{j,n+1} \delta_{j,l+1} + \delta_{j,n-1} \delta_{j,l-1}) - \frac{c_j}{2} (\delta_{j,l} \delta_{j,n+1} + \delta_{j,l} \delta_{j,n-1} + \delta_{j,n} \delta_{j,l+1} + \delta_{j,n} \delta_{j,l-1}) \right) u_l \\
&= -\sum_{l=1}^N \left((c_n^2 + 1) \delta_{n,l} - \frac{1}{2} \sum_{j=1}^N c_j (\delta_{j,l} \delta_{j,n+1} + \delta_{j,l} \delta_{j,n-1} + \delta_{j,n} \delta_{j,l+1} + \delta_{j,n} \delta_{j,l-1}) \right) u_l \\
&= -\sum_{l=1}^N \left((c_n^2 + 1) \delta_{n,l} - \frac{1}{2} (c_l \delta_{l,n+1} + c_l \delta_{l,n-1} + c_n \delta_{n,l+1} + c_n \delta_{n,l-1}) \right) u_l \\
&= -\left((c_n^2 + 1) u_n - \frac{1}{2} (c_{n+1} u_{n+1} + c_{n-1} u_{n-1} + c_n u_{n-1} + c_n u_{n+1}) \right) \\
&= -(c_n - 1)^2 u_n + \left(\frac{c_{n+1} + c_n}{2} u_{n+1} - 2c_n u_n + \frac{c_n + c_{n-1}}{2} u_{n-1} \right) \\
\Rightarrow \ddot{u}_n &= -(c_n - 1)^2 u_n + c_n (u_{n+1} - 2u_n + u_{n-1}) + \frac{c_{n+1} - c_n}{2} u_{n+1} - \frac{c_n - c_{n-1}}{2} u_{n-1} \tag{C6}
\end{aligned}$$

Using the above equation of motion, we will show that at an interface between topologically distinct lattices, i.e. where c crosses 1, irrespective of whether the interface is smooth or sharp, a soft mode localized at the interface always exists when the values of c on either side of the interface are symmetric about 1, i.e. when the values of c on either side sum to 2. For the general case of an interface where c crosses 1, but is not symmetric about 1 on either side, we will solve for the conditions for the existence of localized soft modes, for both smooth and sharp interfaces.

We will treat the case of the smooth and sharp interface separately, beginning with a sharp interface.

1. Sharp Interface

We consider a sharp interface between a lattice with uniform $c = c_L$ on the left and $c = c_R$ on the right. For the bulk regions on either side, writing $u_n(t) = u_0 z^n e^{i\omega t}$, where u_0 is the displacement at the site closest to the interface, the equation of motion: Eq. (C6) becomes:

$$\begin{aligned}
-\omega^2 u_0 z^n &= -(c-1)^2 u_0 z^n + c u_0 z^n (z - 2 + z^{-1}) \\
\Rightarrow \omega^2 &= (c-1)^2 - c(z + z^{-1} - 2) \\
\Rightarrow \omega^2 &= (c_L - 1)^2 - c_L(z_L + z_L^{-1} - 2) \tag{C7}
\end{aligned}$$

$$\Rightarrow \omega^2 = (c_R - 1)^2 - c_R(z_R + z_R^{-1} - 2) \tag{C8}$$

where z_L, z_R are complex numbers describing the growth, decay or oscillatory nature of the mode to the left and right of the interface depending on whether $|z_{L(R)}|$ is greater than, less than, or equal to 1.

Labeling the displacements at the sites adjacent to the interface as $u_{0,L}$ on the left, and $u_{0,R}$ on right, and rewriting Eq. (C6) for these sites, we get:

$$\omega^2 u_{0,L} = (c_L - 1)^2 u_{0,L} - c_L ((z_L^{-1} - 2) u_{0,L} + u_{0,R}) - \frac{c_R - c_L}{2} u_{0,R} \tag{C9}$$

$$\omega^2 u_{0,R} = (c_R - 1)^2 u_{0,R} - c_R ((z_R - 2) u_{0,R} + u_{0,L}) + \frac{c_R - c_L}{2} u_{0,L} \tag{C10}$$

Substituting for ω^2 from Eq.s (C7),(C8) into Eq.s (C9),(C10), we get:

$$c_L z_L u_{0,L} - c_L u_{0,R} - \frac{c_R - c_L}{2} u_{0,R} = 0 \quad (C11)$$

$$c_R z_R^{-1} u_{0,R} - c_R u_{0,L} + \frac{c_R - c_L}{2} u_{0,L} = 0 \quad (C12)$$

For a non-trivial solution to exist for Eq.s (C11),(C12), the following determinant must vanish:

$$\det \begin{pmatrix} c_L z_L & -\frac{c_R + c_L}{2} \\ -\frac{c_R + c_L}{2} & c_R z_R^{-1} \end{pmatrix} = 0$$

$$\Rightarrow \frac{z_L}{z_R} = \frac{(c_R + c_L)^2}{4 c_R c_L} \quad (C13)$$

Notice from Eq. (C13) that $z_L/z_R - 1 > 0 \Rightarrow z_L/z_R > 1$.

We now have three equations: Eq.s (C7),(C8),(C13) for three variables: z_R, z_L, ω^2 .

Subtracting Eq. (C7) from Eq. (C8), eliminates ω^2 and gives:

$$(c_R - 1)^2 - (c_L - 1)^2 - c_R(z_R + z_R^{-1} - 2) + c_L(z_L + z_L^{-1} - 2) = 0$$

$$\Rightarrow (c_R^2 - c_L^2) - c_R(z_R + z_R^{-1}) + c_L(z_L + z_L^{-1}) = 0 \quad (C14)$$

Using Eq. (C13) to eliminate z_L in favor of z_R , we can solve for z_R as follows:

$$(c_R^2 - c_L^2) - c_R(z_R + z_R^{-1}) + c_L \left(\frac{(c_L + c_R)^2}{4 c_L c_R} z_R + \frac{4 c_L c_R}{(c_L + c_R)^2} z_R^{-1} \right) = 0$$

$$\Rightarrow \left(1 - \frac{(c_L + c_R)^2}{4 c_R^2} \right) z_R^2 - \frac{c_R^2 - c_L^2}{c_R} z_R + \left(1 - \frac{4 c_L^2}{(c_L + c_R)^2} \right) = 0$$

$$\Rightarrow z_R = \frac{\frac{c_R^2 - c_L^2}{c_R} \pm \sqrt{\left(\frac{c_R^2 - c_L^2}{c_R} \right)^2 - 4 \left(1 - \frac{(c_L + c_R)^2}{4 c_R^2} \right) \left(1 - \frac{4 c_L^2}{(c_L + c_R)^2} \right)}}{2 \left(1 - \frac{(c_L + c_R)^2}{4 c_R^2} \right)} \quad (C15)$$

Substituting the values for z_R from Eq. (C15) into Eq. (C13) solves for z_L , and substitution into Eq. (C8) solves for ω^2 .

For the solution to be a localized interface mode, it must be growing on the left side: $|z_L| > 1$ and decaying on the right side: $|z_R| < 1$. In the region of parameter space $0 < c_L, c_R < 2$, the values of $\{c_L, c_R\}$ which give localized interface modes are plotted in Fig. 3(d) of the main text.

For the case when c_L, c_R are symmetric about 1, taking $c_L = 1 - m_0$, $c_R = 1 + m_0$, we get the following values for z_R, z_L, ω^2 :

$$z_R = \frac{(1 + m_0)(2 - m_0)}{2 + m_0}, \quad z_L = \frac{2 - m_0}{(2 + m_0)(1 - m_0)}, \quad \omega^2 = m_0^2 - \frac{m_0^4}{4 - m_0^2} \quad (C16)$$

The above values of the mode growth/decay rates and the mode energy are confirmed numerically.

2. Smooth Interface

For a smooth interface, we take the continuum limit of Eq. (C6) with $u_n(t) \rightarrow u(x, t)$. Assuming $u(x, t) = u(x) e^{i\omega t}$, $\ddot{u}(x, t) = -\omega^2 u(x) e^{i\omega t}$, Eq. (C6) becomes:

$$-\omega^2 u(x) = -(c(x) - 1)^2 u(x) + c(x) u''(x) + c'(x) u'(x) \quad (C17)$$

Taking $c(x) = 1 + m(x)$, and working in the limit where $m(x) \ll 1$, the above continuum equation of motion becomes:

$$-\omega^2 u(x) \approx -m^2(x) u(x) + u''(x)$$

$$\Rightarrow u'' + (\omega^2 - m^2(x)) u = 0 \quad (C18)$$

which can be mapped to the time-independent Schrödinger equation:

$$\psi'' + \frac{2m}{\hbar^2}(E - U(x))\psi = 0 \quad (\text{C19})$$

with $\frac{2m}{\hbar^2} = 1$, and $E - U(x) = \omega^2 - m^2(x)$.

At a smooth interface where $c(x)$ crosses 1, the potential energy given by $m^2(x)$ drops down smoothly to 0 at the interface and climbing up to the bulk values of $(c - 1)^2$ on either side of the interface. Hence, a smooth interface between topologically distinct lattices implies a potential well at the interface in the above mapping between Eq. (C18) and Eq. (C19), since $c(x)$ must cross 1 at such an interface. When the asymptotic values of the potential well on the two sides are equal, at least one bound state solution for the Schrödinger equation, Eq. (C19), exists irrespective of the depth of the potential well as shown in [54]. However, when the potential well is asymmetric, i.e. the asymptotic values of the potential energy on either side of the well are unequal, an approximate criterion for a bound state to exist is given by [54] as:

$$W V_0 \gtrsim \sqrt{2\Delta V} \quad (\text{C20})$$

where W is the width of the potential well, V_0 is the depth of the potential well with respect to average of the potential energy on either side of the well, and ΔV is the difference between the potential energies on either side of the well.

Using the above criterion, a localized soft mode at a smooth interface where c crosses 1 exists when

$$W \frac{m_L^2 + m_R^2}{2} \gtrsim \sqrt{2|m_L^2 - m_R^2|} \quad (\text{C21})$$

where m_L^2, m_R^2 are the bulk values of $m^2(x) = (c(x) - 1)^2$ on the left and right sides of the interface, and W is the width of the region over which $c(x)$ varies. The region of parameter space specified by Eq. (C21) is plotted in Fig. 4(e) of the manuscript.

An explicit example of a mapping between Eq. (C18) and Eq. (C19) is possible for $m(x) = m_0 \tanh(x/W)$, where the width of the potential well $m^2(x) = m_0^2 (1 - 1/\cosh^2(x/W))$ is given by W . Since $m^2(x) = m_0^2 (1 - 1/\cosh^2(x/W))$, the equation of motion becomes:

$$u''(x) + \left((\omega^2 - m_0^2) + \frac{m_0^2}{\cosh^2(x/W)} \right) u(x) = 0 \quad (\text{C22})$$

which can be mapped to the Schrödinger equation with $E = (\omega^2 - m_0^2)$, and the potential $U(x) = -m_0^2/\cosh^2(x/W)$.

The number of localized modes, i.e. with $E < 0$, or equivalently with $\omega^2 < m_0^2$ is given by $\lfloor s(m_0, W) \rfloor + 1$, where $s(m_0, W) = \frac{-1 + \sqrt{1 + (4m_0^2 W^2)}}{2}$.

The eigenvalues of the dynamical matrix for the localized modes are given by $\omega_n^2 = m_0^2 - (s(m_0, W) - n)^2/W^2$, for $n = 0, 1, 2, \dots, \lfloor s \rfloor$.

The localized eigenmodes are given by:

$$u_n(x) = \left(1 - \tanh^2\left(\frac{x}{W}\right) \right)^{\frac{s(m_0, W) - n}{2}} {}_2F_1 \left[-n, 2s(m_0, W) + 1 - n; s(m_0, W) - n + 1; \frac{1}{2}(1 - \tanh \frac{x}{W}) \right] \quad (\text{C23})$$

Note that $m_0 \rightarrow 0, W \sim 1 \Rightarrow s \rightarrow 0^+$, and the analytical form of the localized eigenmodes approaches ${}_2F_1[0, 1; 1; \frac{1}{2}(1 - \tanh(x/W))]$ which is a flat line, i.e. a fully delocalized mode.

Examining the regions of parameter space where this approximation breaks:

1. Large m_0 ($m_0 \gtrsim 1$).

The approximation required to arrive at Eq. (C18) is no longer valid, since the neglected term mu'' is now comparable to the retained term u'' . The number of predicted localized modes and the shape of the predicted localized modes are no longer in agreement with the numerically calculated modes, however the numerically calculated lowest energy modes are localized at the interface.

2. Narrow interface ($W \sim 1$).

Even though interface between the topologically distinct bulk phases is now much sharper, where the continuum approximation is not expected to hold, the numerically calculated localized modes match the analytically predicted modes. As $m_0 \rightarrow 0$, both the numerically calculated modes and the analytically predicted modes become delocalized.